

# Systematic calculation of molecular vibrational spectra through a complete Morse expansion.

Andrea Bordoni and Nicola Manini  
*Dipartimento di Fisica, Università di Milano,  
Via Celoria 16, 20133 Milano, Italy*

June 19 2006

## Abstract

We propose an accurate and efficient method to compute vibrational spectra of molecules, based on exact diagonalization of an algebraically calculated matrix based on powers of Morse coordinate. The present work focuses on the 1D potential of diatomic molecules: as typical examples, we apply this method to the standard Lennard-Jones oscillator, and to the *ab-initio* potential of the H<sub>2</sub> molecule. Global cm<sup>-1</sup> accuracy is exhibited through the H<sub>2</sub> spectrum, obtained through the diagonalization of a 30 × 30 matrix. This theory is at the root of a new method to obtain globally accurate vibrational spectral data in the context of the multi-dimensional potential of polyatomic molecules, at an affordable computational cost.

Keywords: vibrational spectra, algebraic method, Morse oscillator, anharmonicity.

## 1 Introduction

Extremely accurate rovibrational levels are obtained routinely for polyatomic molecules by modern spectroscopical techniques. Despite intense effort and significant progress, the accuracy and reliability of theoretical calculations is still lagging far behind especially in the region of high overtones. Many present-day quantum-chemical calculations of spectroscopical properties are based on some power expansion of the adiabatic potential energy surface (PES) at its minimum [1, 2, 3, 4]. Accurate treatment of the kinetic and second-order potential term provides the harmonic normal coordinates and

frequencies. Higher-order (cubic, quartic) power corrections usually account for anharmonic effects. The “force field” parameters are often derived by *ab-initio* methods, or adjusted to experimentally observed levels. Either way, simple power terms in the normal coordinates fit very poorly the global shape of the actual adiabatic potential energy surface (PES) away from its minimum [5]. As a result, methods based on such power expansions retain spectroscopical accuracy only up to few thousand  $\text{cm}^{-1}$  [6, 7, 8, 9] in ordinary simple molecules such as  $\text{H}_2\text{O}$ , or  $\text{H}_2\text{C}_2$ ; the accuracy rapidly deteriorates in the spectral region where dissociation is approached.

To improve this situation, expansions of the PES in suitable internal coordinates [10], for example of the Morse type [11, 12, 13], have been proposed. In this class of schemes, difficulties arise due to the generation and the need to diagonalize very non-sparse matrixes, which impose uncontrolled approximations, involving the neglect of a huge number of matrix elements [14]. To improve this state of affairs here we propose a method, based on the Morse oscillator, which combines the accuracy of a theory which includes anharmonicity right from the start with the simplicity of the harmonic expansion (basis completeness, simple algebraic rules for the matrix elements, sparse coupling matrixes). The present work focuses on the one-dimensional (1D) potential, representing diatomic molecules. In this context where trivial exact numerical solution of the vibrational problem is available, the theory is formulated in its full detail, and its accuracy is tested against the PES of realistic diatomic potentials. This theory is constructed with careful attention to make it suitable as the basic building block for the successive extension to the multi-dimensional potentials of polyatomic molecules, which will be the subject of future work.

Section 2 introduces the formalism, whose application is then investigated in Sec. 3. Conclusions are then drawn in Sec. 4.

## 2 The model

The Morse potential was introduced [15] with the purpose of producing an accurate description of typical spectra of diatomic molecules through an analytically solvable Schrödinger problem. Through standard manipulations of the three dimensional (3D) spherical problem, we come to what is usually named Morse equation

$$\hat{H}_M \Psi(x) \equiv \left[ -\frac{\hat{p}_x^2}{2\mu} + V_M(x) \right] \Psi(x) = W \Psi(x), \quad (1)$$

where  $\mu$  is the reduced molecular mass, and the *Morse Potential* function

$$V_M(x) \equiv V_0 \{ [v(x)]^2 - 1 \}, \quad \text{with } v(x) = e^{-\alpha(x-x_0)} - 1. \quad (2)$$

This potential function is parameterized by the three quantities  $V_0$  (depth of the well),  $\alpha$  (shape parameter), and  $x_0$  (position of the minimum).  $V_M$  reflects the main features of a diatomic molecular potential, namely one well defined minimum, a finite dissociation energy for large  $x$ , a strongly repulsive region at  $x \ll x_0$ , a finite number  $L$  of bound states and a continuum of scattering states. The Morse potential represents an intrinsically anharmonic oscillator, and indeed it was introduced originally to deal with anharmonicity exactly: it has the great advantage that the corresponding Schrödinger equation (1) is solvable exactly in 1D, and approximately when it represents the radial equation of a 2-3D problem.

In terms of the dimensionless parameter

$$s = \frac{\sqrt{2mV_0}}{\hbar\alpha} - \frac{1}{2}, \quad (3)$$

the bound-state eigenfunctions can be written as

$$\Psi_n(x) = N_n e^{-y(x)/2} y(x)^{s-n} L_n^{2(s-n)}(y(x)), \quad (4)$$

where

$$y(x) = (2s + 1) e^{-\alpha(x-x_0)}. \quad (5)$$

$L_n^\mu(z) = \frac{e^z z^{-\mu}}{n!} \frac{d^n}{dz^n} (z^{\mu+n} e^z)$  is a generalized Laguerre polynomial, and

$$N_n = \alpha^{1/2} \left[ \frac{\Gamma(2s - n + 1)}{2(s - n)\Gamma(n + 1)} \right]^{\frac{1}{2}} \quad (6)$$

is a normalization constant. For integer  $n = 0, 1, 2, \dots [s]$  ( $[s]$  indicates the largest integer  $\leq s$ ), the square-integrable wavefunctions  $\Psi_n(x)$  represent the  $[s] + 1$  bound states, for the specific physical parameters of the system. The corresponding energy eigenvalues are

$$W_n(x) = -\frac{\alpha^2 \hbar^2}{2\mu} (s - n)^2. \quad (7)$$

In addition to its many advantages, the Morse potential has a few drawbacks: mainly, it does not approach the dissociation limit (here  $E = 0$ ) with a power law as realistically expected, and it does not quite diverge at  $x = 0$ . On the other hand, a more realistically accurate potential  $V(x)$  can be obtained by adding a suitable correction  $V_d(x) \equiv V(x) - V_M(x)$  to the

starting Morse potential. This correction is often written as an expansion, whose detailed form is determined according to some convenient recipe. Several approaches in this direction are documented in the literature, from the perturbed Morse oscillator model (PMO) [16, 17, 18], to models based on algebraic methods [19, 20, 21]. The PMO approach is based on an expansion of  $V_d(x)$  in a power series of  $v(x)$

$$V_d(x) = \sum_{i=4} a_i [v(x)]^i, \quad (8)$$

then treated perturbatively. In contrast, algebraic approaches based on dynamical symmetries lead to an expansion of the Casimir operator of a Lie group, representing the whole Morse Hamiltonian [19, 20, 21, 22]. Unfortunately, as this operator is of mixed kinetic and potential character, it is hard to relate this second type of expansion to a well defined molecular problem.

Here we propose a substantial improvement of the PMO. This method is based on an expansion of the form

$$V_d(x) = \sum_{i=3}^{N_{max}} a_i [v(x)]^i, \quad (9)$$

including powers of  $v(x)$  up to order  $N_{max}$ , usually a small integer, e.g. 4 or 10. The differences with the PMO are two: (i) the inclusion of the  $[v(x)]^3$  term, which the PMO approach must omit due to the need to limit the number of low-order terms contributing to that perturbative scheme, and which allows much better flexibility and accuracy, as shown in Sec. 3; (ii) the exact, rather than perturbative solution of the resulting quantum mechanical problem. To this respect, the implementation of algebraic rules for the calculation of the matrix elements allows us to treat the third-order term on the same footing as all other terms in  $V_d$ : we compute their matrix elements, and subsequently diagonalize a sparse matrix.

The choice (9) of the form of the potential correction realizes a satisfactory compromise between the quest of a locally accurate parameterization of the target potential  $V(x)$  by means of a globally meaningful expansion, and the need of analytical expressions of its matrix elements. In particular, the expansion (9) satisfies the minimal requirement of being lower-bounded everywhere, provided that the last coefficient  $a_{N_{max}}$  is positive. This feature holds independently of  $N_{max}$ , in contrast to the traditional expansion in powers of  $x$  where the truncation to odd  $N_{max}$  leads to lower-unbounded potentials regardless of the sign of the coefficients [5]. We will show in specific applications that the chosen form (9) is sufficiently flexible to approximate a realistic molecular potential  $V(x)$  substantially better than  $V_M(x)$ , and,

as long as  $V(x)$  is not ill behaved, in principle arbitrarily well on a very wide energy range from the bottom of the well to dissociation. The Morse parameters and the coefficients  $a_i$  are determined by fitting the computed adiabatic potential  $V(x)$ , thus leading to a fully *ab-initio* method to compute the molecular vibrational spectra, as demonstrated in a few examples in Sec. 3. Once the parameters are determined, by taking advantage of the algebraic properties of  $V_d(x)$ , in Sec. 2.1 we build the explicit matrix representation of the Hamiltonian

$$H = H_M + V_d(x) \quad (10)$$

on a variational basis. We then perform a full diagonalization, thus obtaining eigenvalues and eigenfunctions for this quantum mechanical problem. In Sec. 2.1 we consider the basis of Morse eigenstates (4). In Secs. 2.3 and 2.4, we introduce an extended basis, capable to include states in the continuum, thus improving the variational convergency of the vibrational states close to molecular dissociation.

## 2.1 Matrix elements on Morse basis

The expression of the matrix elements of an operator of the form  $[e^{-\alpha(\hat{x}-x_0)}]^t$ , such as appears in power terms  $[\hat{v}(x)]^i = [e^{-\alpha(\hat{x}-x_0)} - 1]^i$ , Eq. (9), on the Morse basis (4) are available in the literature [23]. For convenience we report here the analytical expression for these matrix elements computed by exploiting basic properties of Laguerre polynomials:

$$\begin{aligned} \langle n | [e^{-\alpha(\hat{x}-x_0)}]^t | m \rangle &= \frac{(-1)^{n+m}}{(2s+1)^t} N_n N_m \Gamma[2s - m - n + t] \times \\ &\sum_{\ell=0}^{\min(n,m)} \binom{n-m-1+t}{n-\ell} \binom{m-n-1+t}{m-\ell} \binom{2s-1-m-n+\ell+t}{\ell}, \end{aligned} \quad (11)$$

where  $N_n, N_m$  are the normalization constants of Eq. (6)<sup>1</sup>. The matrix elements of a term  $\hat{v}(x)^i$ , are obtained by combining expressions of this kind. Note that the matrix element (11) is non vanishing for any  $n, m$ : therefore the resulting matrix is not sparse. Equation (11) permits to construct the matrix representation of the Hamiltonian (10), which is exact within the space of Morse bound states. The molecular problem is thus reduced to the diagonalization of a  $([s] + 1) \times ([s] + 1)$  matrix: clearly it yields exact eigenvalues and eigenvectors in the trivial limit  $H \rightarrow H_M$  (i.e.  $V_d(x) = 0$ ).

---

<sup>1</sup> Equation (11) holds for real  $t \geq 0$ , but we are interested only in integer  $t$ : in this case, the first non vanishing term occurs for  $\ell = (1 - \delta_{n,m}) \max(0, \min(n, m) + 1 - t)$ .

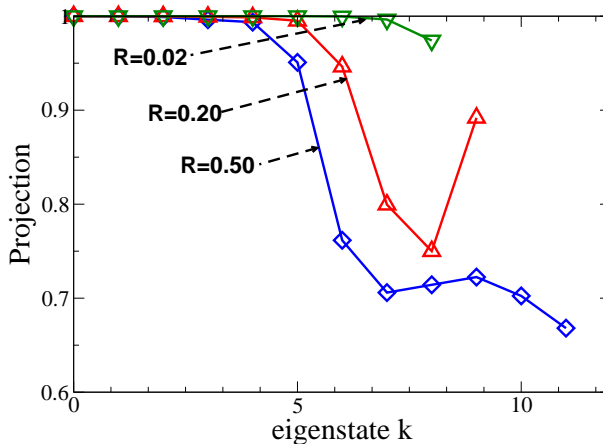


Figure 1: The projection  $\sum_{j=0}^{[s]} |\langle \psi_j | \varphi_k \rangle|^2$  of the  $k^{\text{th}}$  eigenstate on the subspace spanned by the Morse basis, for increasing relative importance  $R$  of the deformation  $V_d(x)$  added to a Morse potential characterized by  $[s] + 1 = 9$  bound states ( $\hbar = \mu = 1$ ,  $s = 8.34$ ).

When  $V_d(x) \neq 0$ ,  $H$  mixes states within the Morse basis to states orthogonal to it. The matrix representation of  $H$  is therefore only approximate, and provides a variational estimate of the energy of the lowest bound states. Due to the imperfect overlap of the subspace of Morse bound states to the subspace of exact bound states of  $H$ , we expect that when the correction  $V_d(x)$  to the Morse problem becomes important in Eq. (10), the accuracy of the description deteriorates. This point is studied in detail in the next section.

## 2.2 The incompleteness of the Morse basis

Morse potential bound states are clearly incomplete for generating the full infinite-dimensional Hilbert space: the un-normalizable wavefunctions of the continuum should also be included to complete it. We expect that the incomplete Morse basis should provide a good description of the actual spectrum for potentials weakly deformed from the Morse shape (small coefficients  $|a_i| \ll V_0$ ), especially for the lowest bound states. For substantial distortion from the Morse shape, the incomplete basis could fail badly, especially for states close to dissociation, and even for intermediate levels.

The incompleteness problem is illustrated quantitatively in Fig. 1, which reports the total projection  $\sum_{j=0}^{[s]} |\langle \psi_j | \varphi_k \rangle|^2$  of the finite-differences numerical eigensolutions  $\varphi_k(x)$  of the Schrödinger equation associated to the potential  $V(x) = V_M(x) + a_4 [v(x)]^4$  to the Morse basis (4). As expected, the projection

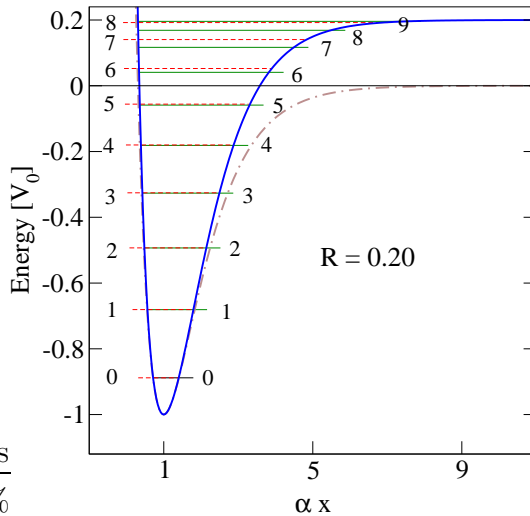


Figure 2: The Schrödinger bound states of the anharmonic oscillator of potential energy  $V(x) = V_M(x) + [v(x)]^4$  (solid curve). Comparison between exact eigenenergies  $E_k^{ex}$  (solid levels) and eigenvalues  $E_k^{alg}$  obtained by diagonalization of the  $H$  matrix within the Morse incomplete subspace (dashed levels). The good accuracy of the lowest levels deteriorates for those close to dissociation, and in particular the highest bound state  $n = 9$  is obviously missing. The pure Morse well  $V_M(x)$  is also outlined for comparison (dot-dashed curve).

of the exact eigenstates of  $H$  on the subspace spanned by the Morse basis (4) gradually reduces from unity (especially for the highest excited states) as the relative weight

$$R = \frac{1}{V_0} \sum_{i=3}^{N_{max}} |a_i| \quad (12)$$

(here  $R = a_4/V_0$ ) of  $V_d(x)$  increases. The increase in well depth caused by increasing  $R$  produces an increase in the number of bound states from 9 (pure Morse), to 12, for  $R = 0.5$ , and this makes the problem of overlaps even more severe. Note that the lowest eigenvectors retain a projection near unity even for large  $R$ . This indicates that the lowest states are determined fairly accurately even within the substantially incomplete basis of a strongly deformed Morse oscillator. In contrast, the accuracy of the states close to dissociation deteriorates rapidly.

Figure 2 illustrates the effect of basis incompleteness on the approximate eigenenergies  $E_k^{alg}$  obtained by numerical diagonalization of the matrix representation of  $H$ , obtained by applying Eqs. (7) and (11). As the overlap

analysis suggests, low levels remain accurate, while close to dissociation the method relying on the Morse basis gives very poor results.

The above calculations focus on the case  $V_d(x) \propto [v(x)]^4$ . A similar analysis can be carried out for any term  $[\hat{v}(x)]^i$  or linear combination thereof, with the same definition (12) for  $R$  and qualitatively similar results.

### 2.3 Beyond the Morse basis

To improve the accuracy of the exact diagonalization method close to dissociation, it is necessary to apply it on a basis which can be systematically enlarged virtually to cover the entire Hilbert space. In recent years, much work has been done to treat at least in an approximate manner the continuum part of the spectrum, mostly in the context of molecules. The main reason is that energy regions near dissociation are becoming available experimentally: in such regions the interaction between the highest-energy bound states and the lowest-energy section of the continuum spectrum is supposed crucial. The quest for manageable approximations of the continuum spectrum has followed different routes, including analytical methods (wavefunctions manipulation in coordinate representation [24, 25]), to essentially algebraic treatments related to the dynamical-symmetry viewpoint [26] or of supersymmetric (SUSY) quantum mechanics derivation [27].

An algebraic approach is the most suited for a subsequent generalization to potentials of the kind of Eq. (9). Moreover, if an algebraic form of the dynamical variables is available, the computation of matrix elements and other interesting quantities can be done by exploiting simple algebraic relations. We sketch here the main ideas followed in the literature, with particular attention to what is useful for our specific work.

The basic idea is to build appropriate generalized ladder operators connecting the different wavefunctions of a given family, and subsequently express all relevant quantities in terms of these operators. The ladder operators on one side allow the identification of the dynamical symmetry of the physical model under consideration, and on the other side lead to an algebraic expression for all relevant dynamical variable, including the Hamiltonian. A similar construction was made for the Morse potential [28], starting from the Morse bound-state eigenfunctions (4).

Eventually, we need a basis where suitable ladder operators act: this basis must be complete in  $\mathcal{L}^2[(0, \infty), dy/y]$ . To this purpose we introduce the following family of wavefunctions [26]

$$\phi_n^\sigma(y) = \sqrt{\frac{\alpha n!}{\Gamma(2\sigma + n)}} y^\sigma e^{-\frac{y}{2}} L_n^{2\sigma-1}(y), \quad n = 0, 1, 2, \dots \quad (13)$$

labeled by a real parameter  $\sigma > 0$ . Following Ref. [29], we refer to  $|\phi_n^\sigma\rangle$  as *quasi number state*. Formally, these functions resemble Morse bound states (4). However they are substantially different. In particular for any  $\sigma > 0$ , the quasi number states do form a complete orthonormal set in  $\mathcal{L}^2[(0, \infty), dy/y]$  [26]. This same set was introduced in Ref. [29], on the basis of considerations related to SUSY quantum mechanics, and applied to the context of molecular spectra in Ref. [30, 31].

The construction of generalized ladder operators realized for Morse bound states can be repeated starting from Eq. (13) [26]. The three resulting operators are

$$\begin{aligned}\hat{K}_- &= (\sigma\hat{I} + \hat{n}) - \frac{\hat{y}}{2} - y\frac{d}{dy} && \left( = (\sigma\hat{I} + \hat{n}) - \frac{\hat{y}}{2} + \frac{i}{\hbar\alpha}\hat{p}_x \right) \\ \hat{K}_+ &= (\sigma\hat{I} + \hat{n}) - \frac{\hat{y}}{2} + y\frac{d}{dy} && \left( = (\sigma\hat{I} + \hat{n}) - \frac{\hat{y}}{2} - \frac{i}{\hbar\alpha}\hat{p}_x \right) \\ \hat{K}_0 &= \sigma\hat{I} + \hat{n},\end{aligned}\quad (14)$$

where  $\hat{n}\phi_n^\sigma = n\phi_n^\sigma$ .  $\hat{K}_-$ ,  $\hat{K}_+$  and  $\hat{K}_0$  act as generalized step up, step down and number operator repeatedly on the states represented by Eq. (13):

$$\hat{K}_-|\phi_n^\sigma\rangle = C_n|\phi_{n-1}^\sigma\rangle \quad (15)$$

$$\hat{K}_+|\phi_n^\sigma\rangle = C_{n+1}|\phi_{n+1}^\sigma\rangle \quad (16)$$

$$\hat{K}_0|\phi_n^\sigma\rangle = (\sigma + n)|\phi_n^\sigma\rangle, \quad (17)$$

where

$$C_n = \sqrt{n(n + 2\sigma - 1)}. \quad (18)$$

The definition (14) can be inverted, to obtain the operatorial form of momentum and Morse coordinate

$$\hat{p}_x = \frac{i\hbar\alpha}{2}(\hat{K}_+ - \hat{K}_-) \quad (19)$$

$$\hat{y} = 2\hat{K}_0 - (\hat{K}_+ + \hat{K}_-). \quad (20)$$

Accordingly, the whole Hamiltonian (1) may be expressed in algebraic form, as done in Ref. [26]: the matrix elements  $\langle\phi_m^\sigma|\hat{H}_M|\phi_n^\sigma\rangle$  can be computed algebraically. The only non-vanishing matrix elements are those for which  $m = n, n \pm 1$ : the Morse Hamiltonian matrix is tridiagonal on the basis  $|\phi_n^\sigma\rangle$ . All the above properties hold regardless of the value of  $\sigma$ , for which a convenient choice will be made in Sec. 2.4.

An instructive similarity to the algebraic structure of the harmonic oscillator may be obtained by following the SUSY approach: in SUSY quantum mechanics the Morse potential satisfies the condition of being *shape-invariant*,

so that its eigenvalues and eigenvectors can be obtained in algebraic form. This leads to the construction of Morse generalized ladder operators of the form

$$\begin{aligned}\hat{A}(q) &= q\hat{I} - \frac{\hat{y}}{2} + \frac{i}{\hbar\alpha}\hat{p}_x \\ \hat{A}^\dagger(q) &= q\hat{I} - \frac{\hat{y}}{2} - \frac{i}{\hbar\alpha}\hat{p}_x ,\end{aligned}\tag{21}$$

parameterized by the real quantity  $q$ . The Morse Hamiltonian (1) can be expressed in factorized form

$$\hat{H}_M = \frac{\hbar^2\alpha^2}{2\mu}[\hat{A}^\dagger(s)\hat{A}(s) - s^2] ,\tag{22}$$

in terms of the operators of Eq. (21) with  $q = s$ , and the formal analogy with harmonic oscillator algebra is evident. Define  $|\Psi_0^q\rangle$  as the only state annihilated by  $\hat{A}(q)$ :  $\hat{A}(q)|\Psi_0^q\rangle = 0$  [29]. For  $q = s$ ,  $|\Psi_0^q\rangle$  coincides with the ground state of Morse Hamiltonian, Eq. (4). The other excited states can be obtained algebraically as

$$|\Psi_n^s\rangle = F_n \prod_{\ell=1}^n \hat{A}^\dagger(s - n + \ell) |\Psi_0^{s-n}\rangle ,\tag{23}$$

where  $F_n$  are normalization constants. Equation (23) is reminiscent of the ladder representation of the harmonic oscillator with two important differences: (i) the excited state  $|\Psi_n^s\rangle$  is generated starting from the ground state of a *different but related* Morse problem; (ii) the ladder operators involved depends explicitly on the step number.

Due to the particularly simple dependence of the operators  $\hat{A}$ ,  $\hat{A}^\dagger$  on the parameter  $q$ , different choices of the step number  $q$  dependency generate new algebraic families of wavefunctions, which do not coincide with Morse eigenstates, but have similar algebraic properties. In particular, setting  $q = \sigma + n$ , starting from the ket  $|\phi_0^\sigma\rangle \equiv |\Psi_0^s\rangle$  annihilated by  $\hat{A}(\sigma)$ , the following family of wavefunctions is generated:

$$|\phi_n^\sigma\rangle = G_n^\sigma \prod_{\ell=1}^n \hat{A}^\dagger(\sigma - 1 + \ell) |\phi_0^\sigma\rangle ,\tag{24}$$

where  $G_n^\sigma$  are appropriate normalization constants. By comparing Eq. (21) with Eq. (14), the following relations emerge:

$$\begin{aligned}\hat{A}(\sigma + n)\phi_n^\sigma &= \hat{K}_-\phi_n^\sigma \\ \hat{A}^\dagger(\sigma + n)\phi_n^\sigma &= \hat{K}_+\phi_n^\sigma .\end{aligned}\tag{25}$$

This means that, for this special ( $n$ -dependent) choice  $q = \sigma + n$ , the  $\hat{A}$ ,  $\hat{A}^\dagger$  operators assume the structure of the family of ladder operators (21), and the states (24) coincide with those of Eq. (13).

These SUSY considerations allow us to see the complete basis of Eq. (13) as a natural algebraic modification of the Morse basis, with the nontrivial advantage that all matrix element of operators expressed as functions of  $\hat{A}(q)$  and  $\hat{A}^\dagger(q)$  (see Eqs. (19) and (20)) can be computed by purely algebraic means. We will take advantage of this feature in the next section to evaluate the matrix elements of all operators involved in the expansion (9).

## 2.4 Matrix elements on the quasi-number basis

In analogy to Sec. 2.1, we derive algebraic matrix elements of powers of the operators  $e^{-\alpha(\hat{x}-x_0)}$ , which appear in the expansion (9) of  $V_d(x)$ , on the basis (13) of quasi number states. In terms of the operators  $A(q)$ ,  $A^\dagger(q)$  defined in Eq. (21), the Morse variable  $\hat{y}$  and the momentum operator can be written as:

$$\hat{y} = (2s + 1)e^{-\alpha(\hat{x}-x_0)} = 2s\hat{I} - [\hat{A}^\dagger(s) + \hat{A}(s)] \quad (26)$$

$$\hat{p}_x = \frac{\hbar\alpha}{2i} [\hat{A}(s) - \hat{A}^\dagger(s)]. \quad (27)$$

The  $\hat{A}(s)$ ,  $\hat{A}^\dagger(s)$  matrix elements are computed explicitly by observing that  $\hat{A}(s) = \hat{A}(\sigma + n) + (s - \sigma - n)\hat{I}$  (and analogously for  $\hat{A}^\dagger$ ):

$$\begin{aligned} \langle \phi_m^\sigma | \hat{A}(s) | \phi_n^\sigma \rangle &= C_n \delta_{m,n-1} + (s - \sigma - n) \delta_{m,n} \\ \langle \phi_m^\sigma | \hat{A}^\dagger(s) | \phi_n^\sigma \rangle &= C_{n+1} \delta_{m,n+1} + (s - \sigma - n) \delta_{m,n}. \end{aligned} \quad (28)$$

Based on the algebraic relations above, it is straightforward to obtain the matrix elements of all the relevant operators. In particular, the matrix elements of  $\hat{H}_M$  are

$$\begin{aligned} \langle \phi_m^\sigma | \hat{H}_M | \phi_n^\sigma \rangle &= \hbar\alpha \left( \frac{2V_0}{\mu} \right)^{\frac{1}{2}} \frac{1}{(2s+1)} \{ [C_m^2 - s^2 + (m-s+\sigma)^2] \delta_{m,n} \\ &+ (s - \sigma - n) C_m \delta_{m,n+1} + (s - \sigma - m) C_n \delta_{m+1,n} \}. \end{aligned} \quad (29)$$

On the quasi number states basis (QNSB) the Hamiltonian  $\hat{H}_M$  is therefore tridiagonal. In practice, this is a minor drawback with respect to the basis (4) of energy eigenstates, since tridiagonal matrices are diagonalized extremely quickly.

We are now ready to choose the value of the  $\sigma$  parameter: from Eq. (29) it is evident that if  $\sigma - s$  equals a positive integer  $d$ , then the off-diagonal

matrix element  $\langle d|\hat{H}_M|d+1\rangle$  vanishes:  $\sigma$  determines the splitting of the Hamiltonian matrix into two blocks. It is natural to set the integer  $d$  to the number  $[s]$  of Morse bound states, i.e.

$$\sigma = s - [s], \quad (30)$$

so that  $0 < \sigma \leq 1$ . Under this assumption the Hilbert space  $\mathcal{H}$  decomposes into the direct sum of a  $([s] + 1)$ -dimensional  $\mathcal{H}^-$  space (bound states (4)), and an infinite dimensional  $\mathcal{H}^+$  space (Morse continuum spectrum) [29, 26]:

$$\mathcal{H} = \mathcal{H}^- \oplus \mathcal{H}^+ \quad (31)$$

In all the following we stick to the assumption (30).

In the same way of Eq. (29), the matrix elements of  $e^{-\alpha(\hat{x}-x_0)}$  are obtained from Eq. (26):

$$\langle \phi_m^\sigma | e^{-\alpha(\hat{x}-x_0)} | \phi_n^\sigma \rangle = \frac{-C_n \delta_{m,n-1} - C_m \delta_{m,n+1} + 2(s - [s] + n) \delta_{m,n}}{2s + 1}. \quad (32)$$

The matrix of  $e^{-\alpha(\hat{x}-x_0)}$  is also *tridiagonal*. Based on Eq. (32), all matrix elements of every term in the expansion (9) can be computed exactly. It is found in particular that the matrix representing  $[\hat{v}(x)]^i$  is  $(2i+1)$ -band diagonal.<sup>2</sup> For the reader's convenience, explicit expressions of the nonzero matrix elements of the  $\langle \phi_n | [\hat{v}(x)]^i | \phi_m \rangle$  for  $i = 3$  to 6 are collected in Appendix A.

Equation (13) represents also the basis of Morse-oscillator-like functions of Ref. [30, 31], but with an initial choice  $\sigma = \frac{1}{2}[2s] + 1$ . The value of  $\sigma$  changes as  $s$  (taken as a free parameter) is adjusted, but it is generally much larger than the choice of Eq. (30) considered for the QNSB of the present work and yielding  $\sigma < 1$ . As a consequence, the complete set of wavefunctions of Ref. [30, 31] decay much faster in approaching dissociation ( $y \rightarrow 0$ ). This makes convergence of the bound states much slower in that approach, as illustrated in Fig. 3 for the pure Morse case, where our choice Eq. (30) only requires  $N_s = 9$  states to reach full convergence. Similarly slow convergence is observed for the distorted potential of Fig. 2. In addition, the matrix elements at the left hand of Eq. (32) have generally nonzero value for any  $n, m$ , thus leading to the computational overhead of nonsparse matrices.

In summary, the following extremely useful properties characterize the QNSB (13) with the choice  $\sigma = s - [s]$ : (i) the first  $[s] + 1$  states generate the same Hilbert subspace as the Morse basis of bound states; (ii) more states can be included simply, with a systematic improvement of the basis completeness;

---

<sup>2</sup> Like on the Morse basis, also on QNSB matrix elements of  $v(x)^t$  for real  $t$  may be obtained analytically in close form

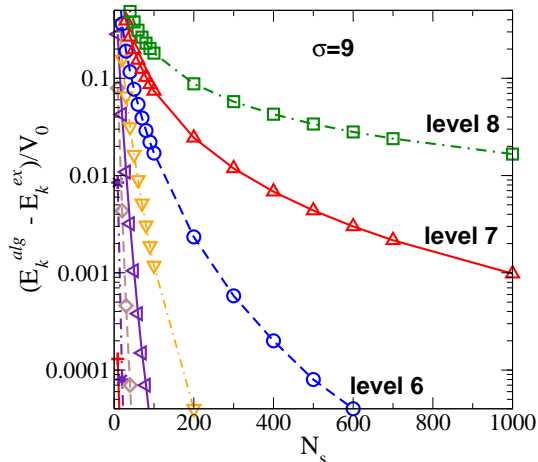


Figure 3: The QNSB with  $\sigma = 9$ , as proposed in Ref. [30, 31]: convergence of the bound eigenenergies of the Morse oscillator of Fig. 1 as the size  $N_s$  of the QNSB (13) increases. This calculation shows that the choice of a value of  $\sigma$  substantially larger than our choice Eq. (30) produces a very slow convergence of the eigenvalues.

(iii) if extended to all  $n \geq 0$ , it becomes to a complete orthonormal basis of  $\mathcal{L}^2[(0, \infty), dy/y]$ , allowing to expand the bound solutions of an arbitrary 1-dimensional problem, with systematically improvable accuracy; (iv) most importantly, it allows to express the matrix elements of all relevant operators in an algebraic form. In particular, the matrix relative to a term  $[\hat{v}(x)]^i$  is  $(2i + 1)$ -band diagonal, so that the finite expansion  $V_d$  and thus  $\hat{H}$  is represented by an extremely sparse matrix, which is even a band matrix! We propose therefore the QNSB as a convenient complete orthonormal system to study the general problem of a molecular oscillator, in a way similar to what is usually done in harmonic expansion methods, but with the advantage of including anharmonicity from the beginning.

## 3 Applications

### 3.1 Convergency with basis extension

Initially we verify that indeed the QNSB realizes basis completion as expected. We start considering the potential of Eq. (9), defined by

$$V_d(x) = RV_0[v(x)]^4 \quad (33)$$

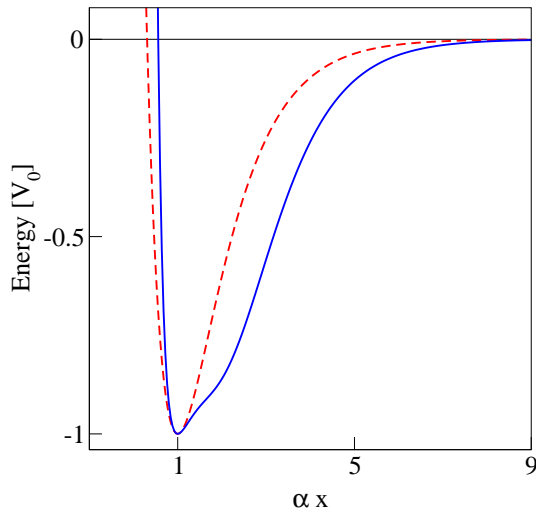


Figure 4: Morse potential (dashed) and potential expansion with  $V_d(x) = 2.0V_0 \sum_{i=3}^6 [v(x)]^i$  (solid).

for  $R = 0.2$ , as in Fig. 2. The eigenvalues  $E_k^{alg}$  of the  $H$ -matrix within the space generated by the first  $N_s$  states in the QNSB converge rapidly to the exact levels  $E_k^{ex}$ , those obtained by the numerical finite-difference integration, represented by solid lines in Fig. 2. The algebraic levels are so accurate that it would be impossible to tell them apart from the solid lines of Fig. 2. As a quantitative measure of the error of the algebraic method, we use a worst-case estimator

$$\Delta_{N_s} := \frac{1}{V_0} \max_k |E_k^{alg} - E_k^{ex}|, \quad (34)$$

which equals  $\Delta_9 = 2.35\%$  for the calculation based on the Morse basis illustrated in Fig. 2. With at least  $N_s = 11$  states included in the QNSB, the bound states reach the correct number of 9 and the  $\Delta_{N_s}$  diminishes fairly rapidly with increasing basis size:  $\Delta_{20} = 0.051\%$ ,  $\Delta_{30} = 0.028\%$ ,  $\Delta_{40} = 0.019\%$ . It is possible to obtain a good accuracy of this method even for large values of  $R$ , namely for potentials significantly distorted from the Morse shape. We check that the same form (33) of the potential for  $R = 1$  yields the correct 14 states with an excellent  $\Delta_{30} = 0.013\%$ .

Good convergence against basis completion was verified also in the presence of multiple power terms, with similar results. For example, for  $V(x) = V_M(x) + 2.0V_0 \sum_{i=3}^6 [v(x)]^i$ , strongly distorted from the Morse shape (see Fig. 4), the 11 bound states are also obtained with good accuracy ( $\Delta_{30} = 0.11\%$ ,  $\Delta_{40} = 0.011\%$ ).

Other tests indicate that a  $\Delta_{N_s}$  within a small fraction of percent is nor-

mally realized by including a number  $N_s$  of states about twice the number of bound states. When high powers of  $v(x)$  are included in  $V_d(x)$  with substantial weight, a larger  $N_s$  could be required for the same accuracy. Substantially fewer states can be included if only few low-lying levels are addressed, and on the contrary,  $N_s$  must be substantially increased to reach convergence of the topmost bound state whenever it happens to occur very close to the continuum, thus associated to a very extended wavefunction.

We have therefore established that the method based on the QNSB (13) is reliable and efficient: given an expansion of the actual molecular potential in the form (9), this method provides accurate eigenvalues and eigenstates, regardless of the relative amount of deviation from the pure Morse potential. We come now to the investigation of the flexibility of the expansion (9) to describe realistic potentials. We consider the Lennard-Jones (LJ) potential, and the adiabatic potential of the  $H_2$  molecule.

### 3.2 The Lennard-Jones potential

We probe the ability of the Morse expansion (9) to describe accurately the standard (12, 6) LJ potential

$$V_{LJ}(x) = A_{LJ} \left[ \left( \frac{\Sigma}{x} \right)^{12} - \left( \frac{\Sigma}{x} \right)^6 \right]. \quad (35)$$

Like the Morse potential,  $V_{LJ}$  is a model potential, which however reproduces well the large- $x$  behavior of the actual interatomic adiabatic potential of, e.g., a dimer of noble gas. Due to its power-law dependencies,  $V_{LJ}$  can be considered as an especially “tough” potential to approximate by a series of Morse-like terms.

As the functional form of the target function  $V(x)$  is assigned, it is straightforward to extract a few exact properties, such as well depth and derivatives at the minimum, which can be imposed to the approximating potential  $V_M + V_d$ . Exact equality of these properties can be used to fix a number of constraints among the  $N_{max} + 1$  parameters which determine  $V_M + V_d$ . The choice of the imposed exact equalities leaves some degree of arbitrariness to the fitting scheme. It is possible to enhance global versus local accuracy, by privileging properties such as the well depth, or rather a number of exact derivatives at the minimum. An analysis of this sort was applied in a different related context (Ref. [16]).

To start, we set  $N_{max} = 2$ , i.e.  $V_d = 0$  and analyze the pure Morse potential. By imposing equal position of the minimum, equal well depth, and equal value of the second derivative at the minimum, we fix all three Morse

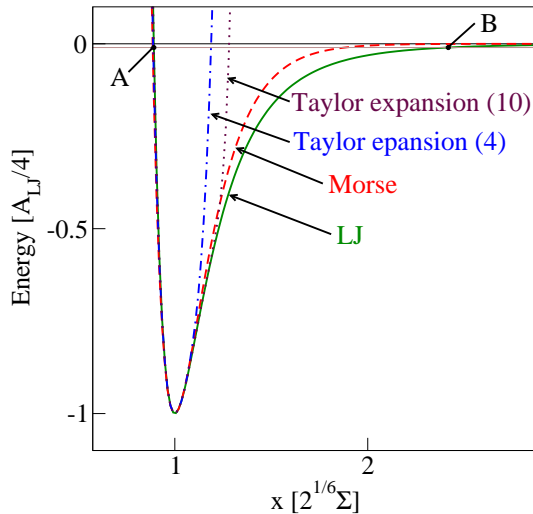


Figure 5: Approximations of the LJ potential (solid): the Morse potential (dashed), with equal position of the minimum, second derivative in the minimum, and well depth; the 4<sup>th</sup> order (dot-dashed) and 10<sup>th</sup> order (dotted) Taylor expansion of  $V_{LJ}$ . The points A and B are characterized by  $V(x) = 1\% V(x_0)$ , i.e. 99% of the dissociation energy from the well bottom.

parameters, and obtain the dashed curve drawn in Fig. 5. These conditions are the natural choice to ensure an overall agreement, which however is not particularly good, as the LJ and Morse potential are the prototypes of two quite different behaviors. As expected, the two potentials differ the most far from the equilibrium distance, in the approach to the dissociation limit.

We then use the full expansion (9) truncated at  $N_{max} = 4$  and  $N_{max} = 6$ . We impose the following conditions: (i) same location of the minimum (fix value of  $x_0$ ), (ii) same values of second and third derivatives at the minimum (fix a relation between  $\alpha$  and  $V_0$ , and a relation involving  $\alpha$  and  $V_0$  and  $a_3$ ), (iii) same well depth (fix  $V_0 + \sum_i (-1)^i a_i$ ). These 4 conditions reduce the number of adjustable parameters to  $N_{max} - 3$ . To determine these residual free parameters, we minimize the RMS difference of  $V(x)$  and  $V_M(x) + V_d(x)$  for approximately  $10^3$  equally spaced  $x$ -points between the points A, B of Fig. 5, where  $V(x) = 1\% V(x_0)$ , i.e. 99% of the dissociation energy measured from the well bottom. The best fit parameters and the corresponding RMS discrepancy of the fit are reported in Table 1. Note that in both calculations the fitting potential is globally well-behaved, as guaranteed by  $a_{N_{max}} > 0$ . The agreement between the target potential  $V_{LJ}$  and the approximating expansion  $V_M + V_d$  is very good already for  $N_{max} = 4$  (one fitted parameter only), and the RMS discrepancy improves by about

	$N_{max} = 4$	$N_{max} = 6$
$\delta_{RMS}$	0.0046	0.00043
$\alpha$	0.10891	0.078138
$V_0$	2.507	4.8698
$a_3$	2.124	7.6676
$a_4$	0.617	5.9625
$a_5$		2.8206
$a_6$		0.6560

Table 1: Best fit parameters in the expansion (9) with  $N_{max} = 4, 6$  to the reference LJ potential with  $\Sigma = 31$ ,  $A_{LJ} = 4$  (so that the well depth is unity).

one order of magnitude for  $N_{max} = 6$  (three fitted parameters). Both fitted potentials are visibly indistinguishable from  $V_{LJ}$ , and have therefore not been drawn in Fig. 5. The fit is essentially independent of the density of the mesh points, except for the choice of the cut at the repulsive side. The 99% of the dissociation is a reasonable compromise to address the bound states.

This accurate fit of  $V(x)$  produces extremely good accord for the corresponding Schrödinger eigenvalues, as shown in Table 2. A fairly accurate spectrum ( $\Delta_{40} = 0.46\%$ ) is obtained already for  $N_{max} = 4$ : the highest eigenvalue is missing but, due to its proximity to dissociation, it is indeed very difficult to determine. The fit with  $N_{max} = 6$  recovers the missing eigenstate, and improves substantially the accuracy of the eigenvalues ( $\Delta_{40} = 0.068\%$ ), determined precisely by the state closest to dissociation. Note that the absolute accuracy of the eigenstates is very close to the accuracy of the underlying functional fit of the potential.

For comparison with the traditional approach, Table 3 lists the exact LJ eigenenergies aside with (i) the approximate spectra computed for the relevant Taylor expansion  $V(x) = \tilde{V}_0 + \sum_{j=2}^{\tilde{N}} c_j (x - x_0)^j$  truncated at  $\tilde{N} = 4$  and 10 (drawn in Fig. 5); (ii) the spectrum obtained by standard second-order perturbation theory applied to the harmonic oscillator, based on the fourth-order Taylor expansion; (iii) the spectrum of the pure Morse term drawn in Fig. 5. It is apparent that the traditional approach can only reach the accuracy of a few percent on few low-lying levels, but fails completely starting already at moderately low overtones. In contrast, even the rough approximation of the pure Morse term provides level estimates within few percent of the  $V_{LJ}$  levels throughout the spectrum. The expanded potential yields a good global description of the spectrum. It would be straightforward to apply the present method to the recently determined adiabatic potential of the  $\text{Ar}_2$  dimer [32], but we prefer to consider in detail a molecule where

$n$	LJ (exact)	$N_{max} = 4$	$N_{max} = 6$
0	-0.88237	-0.88259 (-0.02%)	-0.88240 (-0.002%)
1	-0.67488	-0.67592 (-0.10%)	-0.67494 (-0.006%)
2	-0.50142	-0.50387 (-0.25%)	-0.50146 (-0.004%)
3	-0.35948	-0.36333 (-0.39%)	-0.35942 (0.005%)
4	-0.24637	-0.25098 (-0.46%)	-0.24623 (0.014%)
5	-0.15927	-0.16343 (-0.42%)	-0.15916 (0.011%)
6	-0.09514	-0.09751 (-0.24%)	-0.09520 (-0.006%)
7	-0.05078	-0.05040 (0.04%)	-0.05100 (-0.022%)
8	-0.02278	-0.01973 (0.30%)	-0.02286 (-0.008%)
9	-0.00754	-0.00356 (0.40%)	-0.00711 (0.043%)
10	-0.00126	(missing)	-0.00058 (0.068 %)

Table 2: Bound-state energies for the LJ potential ( $\Sigma = 31$ ,  $A_{LJ} = 4$ ) computed by numeric finite-differences solution of the Schrödinger equation (units of  $\hbar = \mu = 1$ ), compared to the eigenvalues of the problem associated to the best fit  $V_M(x) + V_d(x)$ , solved by diagonalization on the QNSB including  $N_s = 40$  states. All reported figures are significant. In brackets the difference in percent of the well depth  $E_d = A_{LJ}/4$ .

$n$	LJ (exact)	Taylor 4 (exact)	Taylor 4 (pert. theory)	Taylor 10 (exact)	Pure Morse (analytical)
0	-0.8824	-0.8791 (0.3%)	-0.8842 (-0.2%)	-0.8824 (0.001%)	-0.8818 (0.06%)
1	-0.6749	-0.6419 (3%)	-0.6899 (-1.5%)	-0.6742 (0.07%)	-0.6677 (0.7%)
2	-0.5014	-0.3868 (11%)	-0.5588 (-6%)	-0.4913 (1%)	-0.4833 (1.8%)
3	-0.3595	-0.1094 (25%)	-0.5079 (-15%)	-0.3065 (5%)	-0.32862 (3%)
4	-0.2464	(positive	-0.5542 (-30%)	-0.0989 (15%)	-0.20369 (4%)
5	-0.1593	energy	-0.7149 (-55%)	(positive	-0.10850 (5%)
6	-0.0951	...)	...	energy	-0.04304 (5%)
7	-0.0508			...)	-0.00732 (4%)
8	-0.0228				(missing)
9	-0.0075				(missing)
10	-0.0013				(missing)

Table 3: Comparison of the exact  $V_{LJ}$  eigenstates with those of the 4<sup>th</sup> order traditional Taylor expansion (dot-dashed curve in Fig. 5) obtained by exact integration of the differential problem, and by 2<sup>nd</sup> order perturbation theory. The eigenvalues of the pure Morse curve (dashed in Fig. 5) are also reported for comparison. The differences in brackets are in percent of the well depth  $E_d$ .

	Morse	$N_{max} = 4$	$N_{max} = 12$
$\delta_{RMS}$ [Ha]	0.035	0.006	0.00003
$\delta_{RMS}$ [ $\text{cm}^{-1}$ ]	7760	1320	5.5
$\delta_{RMS}/E_d$	0.20	0.03	0.0001
$\alpha$	$1.318 a_0^{-1}$	$1.223 a_0^{-1}$	$0.840657 a_0^{-1}$
$V_0$	0.17447498 Ha	0.120 Ha	0.26147 Ha
$a_3$		-0.030 Ha	0.09233 Ha
$a_4$		0.024 Ha	0.06147 Ha
$a_5$			0.03643 Ha
$a_6$			-0.00995 Ha
$a_7$			-0.02819 Ha
$a_8$			0.04013 Ha
$a_9$			0.02555 Ha
$a_{10}$			-0.04034 Ha
$a_{11}$			0.01243 Ha
$a_{12}$			0.00025 Ha

Table 4: Fit parameters for model potential (9),  $N_{max} = 2, 4, 12$ .

PES is less close to the LJ function.

### 3.3 The H<sub>2</sub> molecule

We acquire the accurate *ab-initio* determination of the H<sub>2</sub> adiabatic potential of Refs. [33]. In our parameterization, we choose to fix both the well depth to the very highly accurate value of  $E_d = 0.17447498$  Ha, and the minimum position  $x_0 = 1.4011 a_0$  [34]. The other  $N_{max} - 1$  parameters, including a constant setting the overall energy zero, are all adjusted by minimization of the RMS deviation  $\delta_{RMS}$  from the *ab-initio* points provided in Ref. [33]. The mesh consists of all 169 available points ranging from  $0.2 a_0$  to  $18 a_0$  representing the effective BO potential for H<sub>2</sub> as computed in Ref. [33]. The fits include all available points. In order to enhance the convergence in the bound-state energy range, the points above 1%  $V(x_0)$  are weighed 1/9 of those in the well region. A first fit with the Morse potential term alone yields a rather poor approximation of  $V_{H_2}$  ( $\delta_{RMS} = 0.035$  Ha), as shown in Fig. 6. We then fit the expansion (9) with  $N_{max} = 4$  and 12, obtaining  $\delta_{RMS} = 0.006$  and 0.00003 Ha respectively. The best fit parameters are listed in Table 4. Figure 6 reports the resulting profiles.

Complete exclusion of the points above 1%  $V(x_0)$  produces better agreement of low-order fits, but makes higher-order fits ( $N_{max} > 8$ ) unstable. On the other hand, enforcing equal accuracy to all points (no weights) makes all

$n$	Ref. [33] cm <sup>-1</sup>	Spline cm <sup>-1</sup>	Pure Morse cm <sup>-1</sup>	Eq. (9) $N_{max} = 4$ cm <sup>-1</sup>	Eq. (9) $N_{max} = 12$ cm <sup>-1</sup>
0	-36118	-36112	-35524 (2%)	-36136 (-0.06%)	-36113 (-0.002%)
1	-31957	-31948	-30298 (4%)	-31963 (-0.04%)	-31948 (-)
2	-28031	-28021	-25488 (7%)	-27979 (0.1%)	-28020 (0.001%)
3	-24336	-24324	-21093 (8%)	-24203 (0.3%)	-24324 (-)
4	-20868	-20854	-17114 (10%)	-20651 (0.5%)	-20856 (-0.004%)
5	-17626	-17612	-13550 (11%)	-17340 (0.7%)	-17614 (-0.005%)
6	-14612	-14598	-10402 (11%)	-14282 (0.8%)	-14599 (-0.004%)
7	-11830	-11815	-7670 (11%)	-11491 (0.8%)	-11815 (-)
8	-9287	-9272	-5353 (11%)	-8979 (0.8%)	-9271 (0.003%)
9	-6994	-6980	-3451 (9%)	-6755 (0.6%)	-6979 (0.003%)
10	-4967	-4955	-1965 (8%)	-4829 (0.3%)	-4955 (-)
11	-3230	-3220	-895 (6%)	-3213 (0.02%)	-3222 (-0.006%)
12	-1816	-1807	-240 (4%)	-1915 (-0.3%)	-1810 (-0.01%)
13	-766	-760	-1. (2%)	-943 (-0.5%)	-761 (-0.002%)
14	-145	-142		-308 (-0.4%)	-135 (0.02%)
15				-7	

Table 5: Comparison of the computed H<sub>2</sub> bound-state energies: Ref. [33] includes nonadiabatic corrections; when these corrections are left out, and all bound states of the splined potential of Ref. [33] are computed by numerical solution of the differential Schrödinger problem, the energies of the second column are obtained. The successive columns report eigenvalues of the pure Morse term and of the expansion (9), fitted to the same adiabatic potential of Ref. [33]. Discrepancies to the energies in the second column are reported in brackets: those of less than 0.001% are replaced by a slash.

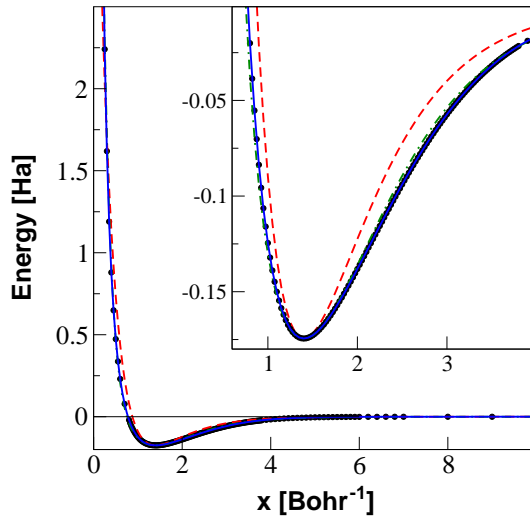


Figure 6: Adiabatic potential for  $\text{H}_2$ , from Ref. [33] (dots). Best fit Morse potential with  $\alpha$  as only adjusted parameter (dashed), and fit function (9), with  $N_{max} = 4$  (dot-dashed) and  $N_{max} = 12$  (solid). Inset: detail of the minimum region, where the small inaccuracy of the dot-dashed curve makes it distinguishable from the solid curve.

fits much less accurate.

The model Hamiltonian is solved on a QNSB including the first  $N_s = 60$  states: the computed levels are summarized in Table 5. The obtained eigenenergies are to be compared with those obtained by numerical integration of the Schrödinger problem of a third-order spline going through the points of Ref. [33]. These reference energies (second column of Table 5) differ from the levels obtained in Ref. [33] in non including the nonadiabatic corrections. The agreement improves systematically as  $N_{max}$  increases, with a worst discrepancy of  $324 \text{ cm}^{-1}$  for  $N_{max} = 4$ , which reduces to  $7 \text{ cm}^{-1}$  for  $N_{max} = 12$ . If the state closest to dissociation is not considered, all other levels are computed within  $2.4 \text{ cm}^{-1}$  of their reference values.

In fact the  $N_{max} = 12$  spectrum could equally well be computed on a QNSB of  $N_s = 30$  states only, and the same  $\text{cm}^{-1}$  figures are obtained. The reason is that the underlying Morse term is so wide and deep that it could host 26 bound states, so that even the pure Morse basis would be almost complete for the bound states of the well at hand. The  $N_{max} = 4$  calculation generates an extra spurious bound state whose precise energy location converges only very slowly with  $N_s$ , while all other states require only  $N_s = 60$  to remain stable to  $\text{cm}^{-1}$ . This is due to the narrow shallow Morse well underlying this expansion. In such a kind of expansion, the QNSB

is absolutely necessary: the Morse basis would produce very poorly converged spectra.

## 4 Discussion and conclusions

In this work we propose a technique to compute molecular vibrational spectra including anharmonic effects using an appropriate virtually complete Hilbert-space basis, the QNSB (13), and a smart prescription for the form of the model potential, namely Eq. (9). The substantial advantage of the proposed combination of Hamiltonian and basis resides in the fully algebraic form of the matrix elements, which can be computed quickly and efficiently, and in the sparse form of the final matrix. The model potential of Eq. (9) is sufficiently flexible to realize a good compromise between local and global accuracy, with relatively low order expansions. In principle, the virtually complete QNSB allows to determine accurate vibrational levels in the whole bound-states energy range, and even to study dissociation phenomena [26, 29].

In the past, a similar approach was applied to restricted forms of the expansion (9). For example, the PMO prescription [16, 17] exclude the  $[\hat{v}(x)]^3$  term and determine the Morse parameters  $\alpha$  and  $V_0$  in order to satisfy the conditions that the second and third derivatives of the two potentials coincide at the minimum. This fixes rigidly the global shape of all other terms, making that expansion much less flexible and accurate. It is eventually still possible to recover a good accuracy in that approximation, but it is necessary to extend the expansion (9) to much higher order. In fact, there is no special reason to fix the pure Morse contribution to some local property of the addressed potential, such as derivatives at the minimum, also because these local properties could even not be available in the realistic case of a microscopic potential derived by *ab initio* numerical calculations.

Other algebraic methods [19, 20, 21, 22] do not rely on an explicit potential, and this makes the calculation of matrix elements of arbitrary operators and roto-vibrational couplings impossible to carry out without the introduction of additional ad hoc parameters. The present method can instead generate all matrix elements of  $\hat{y}^i = e^{-\alpha i \hat{x}}$ , of  $\hat{x}^i e^{-\alpha' \hat{x}}$ , and of  $\hat{p}_x^i$  by straightforward algebraic manipulation.

The method presented here is not the only one to involve smart choices of expansion variables. For example, in the direct-potential-fit methods [35, 36, 37, 38, 39, 40, 41] the roto-vibrational spectroscopy of diatomic molecules is addressed by taking the experimental spectra as input. Nonadiabatic effects can also be included. The validity of the potential parameterization generated by such methods is usually restricted to the energy

range where data are available. The method of the present work generates instead purely vibrational spectra based on first-principle determination of the adiabatic PES, thus with relatively constant accuracy through the whole bound-state energy range. The PES parameterization proposed here is based on *ab-initio* electronic-structure calculations. It would be difficult (and of little interest) to attempt to use the present formalism to fit experimental lines, as in the direct-potential-fit approach. An extension to address nonadiabatic and rovibrational effects could be developed in future work.

When this method is extended to a polyatomic context, the total basis size and its sparseness are the main computational issues to consider. If in the present scheme spectroscopic accuracy can be obtained with as few as 30 states per degree of freedom, the total basis size could still approach  $30^6 \simeq 10^9$  states for a tetraatomic molecule. This size could exceed the computational power available, even if the matrix to diagonalize is sparse. As common practice in quantum chemical calculations, a truncated basis could be selected by accepting slightly less accurate spectra. This truncation may target specific 1D oscillators: in this case, when  $N_s$  is reduced to the number  $[s] + 1$  of the underlying Morse term, the QNSB and the Morse basis are equivalent and yield equivalent spectra. If further reduction is needed, the convergency of the two resulting spectra shows a characteristically different deterioration. Truncation of the Morse basis affects greatly the high-energy states near dissociation: these disappear rapidly one by one, without significant modification of the low-energy levels. On the contrary, the reduction of QNSB size affects eigenenergies throughout the whole spectrum, but with a much slower decrease of the number of bound states. Accordingly, the two basis can be both used with success, keeping in mind their different behavior in different situations. Alternatively, standard truncation of the full many-oscillator basis, based on the relative perturbative weight of the states [5, 42] is also made efficient by the very sparse structure of the matrix elements.

Extension of the method presented here to vibrational spectra of polyatomic molecules is not especially more complicated than the formally similar traditional harmonic-oscillator based expansion. In particular it lends itself naturally to both diagonalization (Lanczos / Davidson) [2, 3, 9, 43] and Green-function-based [4, 5] iterative methods of solution. Special care must be put in making sure that the total polyatomic adiabatic potential surface (e.g. fitted on *ab initio* data) has a single absolute minimum. This global property is easier to implement than on traditional power-series methods where the global shape of the approximate potential is dictated by local properties at the equilibrium geometry. A separate treatment of “soft” torsional coordinates may be needed, exactly like within the traditional normal-coordinate harmonic-oscillator based schemes. Once the extension to the

polyatomic case is realized, the present method will compete successfully with the traditional methods, to yield *ab-initio* vibrational spectra of acceptable accuracy up to the high-overtones near-dissociation energy range.

## A Matrix elements on the QNSB

We report here the nonzero matrix elements of the cubic term  $[\hat{v}(x)]^3$ :

$$\langle \phi_n | [\hat{v}(x)]^3 | \phi_{n-3} \rangle = -\frac{C_{n-2}C_{n-1}C_n}{(1+2s)^3} \quad (36)$$

$$\langle \phi_n | [\hat{v}(x)]^3 | \phi_{n-2} \rangle = \frac{3C_{n-1}C_n(2n-2[s]-3)}{(1+2s)^3} \quad (37)$$

$$\langle \phi_n | [\hat{v}(x)]^3 | \phi_{n-1} \rangle = -\frac{C_n}{(1+2s)^3}(12n^2-24n+13+C_{n-1}^2+C_n^2+C_{n+1}^2) + 12[s]^2-24n[s] \quad (38)$$

$$\langle \phi_n | [\hat{v}(x)]^3 | \phi_n \rangle = \frac{1}{(1+2s)^3}[C_n^2(6n-6[s]-5)+C_{n+1}^2(6n-6[s]-1) + (2n-2[s]-1)^3]. \quad (39)$$

Similarly, the nonzero matrix elements of the quartic term  $[\hat{v}(x)]^4$  read:

$$\langle \phi_n | [\hat{v}(x)]^4 | \phi_{n-4} \rangle = \frac{C_{n-3}C_{n-2}C_{n-1}C_n}{(1+2s)^4} \quad (40)$$

$$\langle \phi_n | [\hat{v}(x)]^4 | \phi_{n-3} \rangle = \frac{8C_{n-2}C_{n-1}C_n(2-n+[s])}{(1+2s)^4} \quad (41)$$

$$\langle \phi_n | [\hat{v}(x)]^4 | \phi_{n-2} \rangle = \frac{C_{n-1}C_n}{(1+2s)^4}(58-72n+24n^2+C_{n-2}^2+C_{n-1}^2+C_n^2) + C_{n+1}^2 + 72[s]-48n[s]+24[s]^2 \quad (42)$$

$$\langle \phi_n | [\hat{v}(x)]^4 | \phi_{n-1} \rangle = -\frac{4C_n}{(1+2s)^4}[-10+26n-24n^2+8n^3-C_{n+1}^2] + 2nC_{n+1}^2 + C_{n-1}^2(2n-3-2[s]) + 2C_n^2(n-1-[s]) - 26[s] + 48n[s] - 24n^2[s] - 2C_{n+1}^2[s] - 24[s]^2 + 24n[s]^2 - 8[s]^3 \quad (43)$$

$$\langle \phi_n | [\hat{v}(x)]^4 | \phi_n \rangle = \frac{1}{(1+2s)^4}\{C_n^4 + C_{n+1}^4 + (1-2n+2[s])^4 + C_{n+1}^2 \times (2-8n+24n^2+C_{n+2}^2 + (8-48n)[s] + 24[s]^2) + C_n^2[C_{n-1}^2 + 2(9-20n+12n^2+C_{n+1}^2 + 20[s]-24n[s]+12[s]^2)]\}. \quad (44)$$

The nonzero matrix elements of the term  $[\hat{v}(x)]^5$  read:

$$\langle \phi_n | [\hat{v}(x)]^5 | \phi_{n-5} \rangle = -\frac{C_{n-4}C_{n-3}C_{n-2}C_{n-1}C_n}{(1+2s)^5} \quad (45)$$

$$\langle \phi_n | [\hat{v}(x)]^5 | \phi_{n-4} \rangle = -\frac{5C_{n-3}C_{n-2}C_{n-1}C_n}{(1+2s)^5} (2n-5-2[s]) \quad (46)$$

$$\begin{aligned} \langle \phi_n | [\hat{v}(x)]^5 | \phi_{n-3} \rangle = & -\frac{C_{n-2}C_{n-1}C_n}{(1+2s)^5} (170-160n+40n^2+C_{n-3}^2 \\ & +C_{n-2}^2+C_{n-1}^2+C_n^2+C_{n+1}^2+160[s]-80n[s]+40[s]^2) \end{aligned} \quad (47)$$

$$\begin{aligned} \langle \phi_n | [\hat{v}(x)]^5 | \phi_{n-2} \rangle = & -\frac{C_{n-1}C_n}{(1+2s)^5} [330-580n+360n^2-80n^3+13C_n^2 \\ & -10nC_n^2+9C_{n+1}^2-10nC_{n+1}^2+580[s]-720n[s]+240n^2[s]+10C_n^2[s] \\ & +10C_{n+1}^2[s]+360[s]^2-240n[s]^2+80[s]^3+C_{n-1}^2(17-10n+10[s]) \\ & +C_{n-2}^2(21-10n+10[s])] \end{aligned} \quad (48)$$

$$\begin{aligned} \langle \phi_n | [\hat{v}(x)]^5 | \phi_{n-1} \rangle = & -\frac{C_n}{(1+2s)^5} [121-400n+520n^2-320n^3+80n^4+C_n^4 \\ & +C_n^4+14C_{n+1}^2-40nC_{n+1}^2+40n^2C_{n+1}^2+C_{n+1}^4+C_{n+1}^2C_{n+2}^2+400[s] \\ & -1040n[s]+960n^2[s]-320n^3[s]+40C_{n+1}^2[s]-80nC_{n+1}^2[s]+520[s]^2 \\ & -960n[s]^2+480n^2[s]^2+40C_{n+1}^2[s]^2+320[s]^3-320n[s]^3+80[s]^4 \\ & +2C_n^2(21-40n+20n^2+C_{n+1}^2-40(n-1)[s]+20[s]^2)+C_{n-1}^2(94 \\ & -120n+40n^2+C_{n-2}^2+2C_n^2+C_{n+1}^2+120[s]-80n[s]+40[s]^2)] \end{aligned} \quad (49)$$

$$\begin{aligned} \langle \phi_n | [\hat{v}(x)]^5 | \phi_n \rangle = & -\frac{1}{(1+2s)^5} \{C_{n+1}^4(1-10n+10[s]) \\ & +C_n^4(9-10n+10[s])+C_{n+1}^2[2-20n+40n^2-80n^3+20(1-4n \\ & +12n^2)[s]-40(6n-1)[s]^2+80[s]^3+C_{n+2}^2(10[s]-3-10n)] \\ & +C_n^2\{C_{n-1}^2(13-10n+10[s])+2[29-90n+100n^2-40n^3 \\ & +10(9-20n+12n^2)[s]-20(6n-5)[s]^2+40[s]^3 \\ & +C_{n+1}^2(5-10n+10[s])\}+(1-2n+2[s])^5\}. \end{aligned} \quad (50)$$

The nonzero matrix elements of the term  $[\hat{v}(x)]^6$  read:

$$\langle \phi_n | [\hat{v}(x)]^6 | \phi_{n-6} \rangle = \frac{C_{n-5}C_{n-4}C_{n-3}C_{n-2}C_{n-1}C_n}{(1+2s)^6} \quad (51)$$

$$\langle \phi_n | [\hat{v}(x)]^6 | \phi_{n-5} \rangle = \frac{12C_{n-4}C_{n-3}C_{n-2}C_{n-1}C_n}{(1+2s)^6} (3-n+[s]) \quad (52)$$

$$\begin{aligned} \langle \phi_n | [\hat{v}(x)]^6 | \phi_{n-4} \rangle &= \frac{C_{n-3}C_{n-2}C_{n-1}C_n}{(1+2s)^6} (395 - 300n + 60n^2 + C_{n-4}^2) \quad (53) \\ &+ C_{n-3}^2 + C_{n-2}^2 + C_{n-1}^2 + C_n^2 + C_{n+1}^2 + 300[s] - 120n[s] + 60[s]^2 \end{aligned}$$

$$\begin{aligned} \langle \phi_n | [\hat{v}(x)]^6 | \phi_{n-3} \rangle &= -\frac{4C_{n-2}C_{n-1}C_n}{(1+2s)^6} [-380 + 510n - 240n^2 + 40n^3] \quad (54) \\ &- 6C_{n-1}^2 + 3nC_{n-1}^2 - 5C_n^2 + 3nC_n^2 - 4C_{n+1}^2 + 3nC_{n+1}^2 + C_{n-3}^2 \times \\ &(-8 + 3n - 3[s]) + C_{n-2}^2(-7 + 3n - 3[s]) - 510[s] + 480n[s] \\ &- 120n^2[s] - 3C_{n-1}^2[s] - 3C_n^2[s] - 3C_{n+1}^2[s] - 240[s]^2 \\ &+ 120n[s]^2 - 40[s]^3 \end{aligned}$$

$$\begin{aligned} \langle \phi_n | [\hat{v}(x)]^6 | \phi_{n-2} \rangle &= \frac{C_{n-1}C_n}{(1+2s)^6} [1771 - 3960n + 3480n^2 - 1440n^3 + 240n^4] \quad (55) \\ &+ C_{n-2}^4 + C_{n-1}^4 + 107C_n^2 - 156nC_n^2 + 60n^2C_n^2 + C_n^4 + 59C_{n+1}^2 - 108nC_{n+1}^2 \\ &+ 60n^2C_{n+1}^2 + 2C_n^2C_{n+1}^2 + C_{n+1}^4 + C_{n+1}^2C_{n+2}^2 + 3960[s] - 6960n[s] \\ &+ 4320n^2[s] - 960n^3[s] + 156C_n^2[s] - 120nC_n^2[s] + 108C_{n+1}^2[s] - 120nC_{n+1}^2[s] \\ &+ 3480[s]^2 - 4320n[s]^2 + 1440n^2[s]^2 + 60C_n^2[s]^2 + 60C_{n+1}^2[s]^2 + 1440[s]^3 \\ &- 960n[s]^3 + 240[s]^4 + C_{n-1}^2(179 - 204n + 60n^2 + 2C_n^2 + C_{n+1}^2 + 204[s] \\ &- 120n[s] + 60[s]^2) + C_{n-2}^2(275 - 252n + 60n^2 + C_{n-3}^2 + 2C_{n-1}^2 + C_n^2 \\ &+ C_{n+1}^2 + 252[s] - 120n[s] + 60[s]^2) \end{aligned}$$

$$\begin{aligned} \langle \phi_n | [\hat{v}(x)]^6 | \phi_{n-1} \rangle &= -\frac{4C_n}{(1+2s)^6} [-91 + 363n - 600n^2 + 520n^3 - 240n^4 + 48n^5] \quad (56) \\ &- 11C_{n+1}^2 + 42nC_{n+1}^2 - 60n^2C_{n+1}^2 + 40n^3C_{n+1}^2 - C_{n+1}^4 + 3nC_{n+1}^4 \\ &+ 3nC_{n+1}^2C_{n+2}^2 + C_{n-1}^4(-5 + 3n - 3[s]) + 3C_n^4(n-1-[s]) - 363[s] \\ &+ 1200n[s] - 1560n^2[s] + 960n^3[s] - 240n^4[s] - 42C_{n+1}^2[s] + 120nC_{n+1}^2[s] \\ &- 120n^2C_{n+1}^2[s] - 3C_{n+1}^4[s] - 3C_{n+1}^2C_{n+2}^2[s] - 600[s]^2 + 1560n[s]^2 - 1440n^2[s]^2 \\ &+ 480n^3[s]^2 - 60C_{n+1}^2[s]^2 + 120nC_{n+1}^2[s]^2 - 520[s]^3 + 960n[s]^3 \\ &- 480n^2[s]^3 - 40C_{n+1}^2[s]^3 - 240[s]^4 + 240n[s]^4 - 48[s]^5 + C_{n-1}^2 \times \\ &[-153 + 282n - 180n^2 + 40n^3 - 3C_{n+1}^2 + 3nC_{n+1}^2 + 2C_n^2(-4 + 3n - 3[s]) \\ &+ 3C_{n-2}^2(n-2-[s]) - 282[s] + 360n[s] - 120n^2[s] - 3C_{n+1}^2[s] - 180[s]^2 + 120n[s]^2 \\ &- 40[s]^3] + 2C_n^2(-23 + 63n - 60n^2 + 20n^3 + C_{n+1}^2(-2 + 3n - 3[s]) \\ &- 3(21 - 40n + 20n^2)[s] + 60(n-1)[s]^2 - 20[s]^3) \end{aligned}$$

$$\begin{aligned}
\langle \phi_n | [\hat{v}(x)]^6 | \phi_n \rangle &= \frac{1}{(1+2s)^6} \{ C_n^6 + C_{n+1}^6 + (1 - 2n + 2[s])^6 + C_{n+1}^4 \{ 2C_{n+2}^2 \quad (57) \\
&+ 3[1 - 4n + 20n^2 + (4 - 40n)[s] + 20[s]^2] \} + C_n^4 [2C_{n-1}^2 + 3(17 - 36n + 20n^2 + C_{n+1}^2 \\
&+ (36 - 40n)[s] + 20[s]^2)] + C_n^2 \{ 179 - 696n + 1080n^2 - 800n^3 + 240n^4 + C_{n-1}^4 \\
&+ 3C_{n+1}^4 + 696[s] - 2160n[s] + 2400n^2[s] - 960n^3[s] + 1080[s]^2 - 2400n[s]^2 \\
&+ 1440n^2[s]^2 + 800[s]^3 - 960n[s]^3 + 240[s]^4 + C_{n-1}^2 (107 - 156n + 60n^2 \\
&+ C_{n-2}^2 + 2C_{n+1}^2 + 156[s] - 120n[s] + 60[s]^2) + 2C_{n+1}^2 [19 - 60n + 60n^2 \\
&+ C_{n+2}^2 - 60(2n - 1)[s] + 60[s]^2] \} + C_{n+1}^2 \{ 3 - 24n + 120n^2 - 160n^3 + 240n^4 \\
&+ C_{n+2}^4 + 24(1 - 10n + 20n^2 - 40n^3)[s] + 120(1 - 4n + 12n^2)[s]^2 - 160(6n - 1)[s]^3 \\
&+ 240[s]^4 + C_{n+2}^2 [11 + 36n + 60n^2 + C_{n+3}^2 - 12(3 + 10n)[s] + 60[s]^2] \} \}.
\end{aligned}$$

## References

- [1] Carter, S.; Bowman, J. M.; Harding, L. B. *Spectrochim. Acta A* 1997, 53, 1179.
- [2] Wyatt, R. J. *Chem. Phys.* 1998, 109, 10732.
- [3] Pochert, J.; Quack, M.; Stohner, J.; Willeke, M. J. *Chem. Phys.* 2000, 113, 2719.
- [4] Stuchebrukhov, A. A.; Marcus, R. A. *J. Chem. Phys.* 1993, 98, 6044.
- [5] Del Monte, A.; Manini, N.; Molinari, L. G.; Brivio, G. P. *Mol. Phys.* 2005, 103, 689.
- [6] Császár, A. G.; Mills, I. M. *Spectrochim. Acta A* 1997, 53, 1101.
- [7] Koput, J.; Peterson, K. A. *Chem. Phys. Lett.* 1998, 283, 139.
- [8] Miani, A.; Hänninen, V.; Horn, M.; Halonen, L. *Mol. Phys.* 2000, 98, 1737.
- [9] Callegari, A.; Pearman, R.; Choi, S.; Engels, P.; Srivastava, H.; Gruebele, M.; Lehmann, K. K.; Scoles, G. *Mol. Phys.* 2003, 101, 551.
- [10] Jensen, P. *Mol. Phys.* 2000, 98, 1253.
- [11] Jensen, P. J. *Mol. Spectrosc.* 1988, 128, 478.
- [12] Lemus, R. J. *Mol. Spectrosc.* 2004, 225, 73.
- [13] Halonen, L.; Carrington Jr, T. J. *Chem. Phys.* 1988, 88, 4171.
- [14] Child, M. S.; Halonen, L. *Adv. Chem. Phys.* 1984, 57, 1.
- [15] Morse, P. M. *Phys. Rev.* 1929, 34, 57.
- [16] Huffaker, J. N. *J. Chem. Phys.* 1976, 64, 3175.
- [17] Huffaker, J. N.; Tran, L. B. *J. Chem. Phys.* 1982, 76, 3838.
- [18] Makarewicz, J. J. *Phys. B: At. Mol. Opt. Phys.* 1990, 24, 383.
- [19] Iachello, F.; Levine, R. D. *Algebraic Theory of Molecules*, Oxford University Press, 1995, p. 161.

- [20] van Roosmalen, O. S. Algebraic Descriptions of Nuclear, Molecular Rotation-Vibration Spectra, PhD Thesis, Univ. Gröningen, 1982, unpublished.
- [21] Oss, S. Adv. Chem. Phys. XCIII, 455.
- [22] Iachello, F.; Levine, R. D. J. Chem. Phys. 1982, 77 , 3046.
- [23] Sage, M. L. Chem. Phys. 1978, 35, 375.
- [24] Pérez-Bernal, F.; Martel, I.; Arias, J. M.; Gómez-Camacho, J. Phys. Rev. A 2001, 63, 052111.
- [25] Pérez-Bernal, F.; Martel, I.; Arias, J. M.; Gómez-Camacho, J. Phys. Rev. A 2003, 67, 052108.
- [26] Lemus, R.; Arias, J. M.; Gómez-Camacho, J. J. Phys. A : Math. Gen. 2004, 37, 1805.
- [27] Cooper, F.; Khare, A.; Sukhatme, U. P. Phys. Rep. 1995, 251, 268.
- [28] Dong, S. H.; Lemus, R. Int. J. Quantum Chem. 2002, 86, 265.
- [29] Molnár, B.; Földi, P.; Benedict, M. G.; Bartha, F. Europhys. Lett. 2003, 61 (4), 445.
- [30] Tennyson, J.; Sutcliffe, B. T. J. Chem. Phys. 1982, 77, 4061.
- [31] Tennyson, J.; Kostin, M. A.; Barletta, P.; Harris, G. J.; Polyansky, O. L.; Ramanlal, J.; Zobov, N. F. Comp. Phys. Comm. 2004, 163, 85.
- [32] Patkowski, K.; Murdachaew, G.; Fou, C.-M.; Szalewicz, K. Mol. Phys. 2005, 103, 2031.
- [33] Schwartz, C.; Le Roy, R. J. J. Mol. Spectrosc. 1987, 121, 420.
- [34] Kolos, W.; Wolniewicz, L. J. Chem. Phys. 1968, 49, 404.
- [35] Ogilvie, J. F. J. Phys. B: At. Mol. Opt. Phys. 1994, 27, 47.
- [36] Ogilvie, J. F. J. Mol. Spectrosc. 1996, 180, 193.
- [37] Coxon, J. A.; Molski, M. Phys. Chem. Comm. 2001, 20, 1.
- [38] Ogilvie, J. F. Chem. Phys. Lett. 2001, 348, 447.
- [39] Coxon, J. A.; Molski, M. Spectrochim. Acta A 2003, 59, 13.

- [40] Coxon, J. A.; Molski, M. J. *Mol. Spectrosc.* 2004, 223, 51.
- [41] Le Roy, R. J. *J. Mol. Spectrosc.* 2004, 228, 92.
- [42] Handy, N. C.; Carter, S. *Mol. Phys.* 2004, 102, 2201.
- [43] Gruebele, M. J. *Chem. Phys.* 1996, 104, 2453.